



Parametric study on non-vacuum chemical vapor deposition of CuInS_2 from a single-source precursor

Christopher V. Kelly^a, Michael H.-C. Jin^{a,b,*}, Kulbinder K. Banger^{a,b},
Jeremiah S. McNatt^b, John E. Dickman^b, Aloysius F. Hepp^{b,*}

^a Ohio Aerospace Institute, Brookpark, OH 44142, USA

^b NASA Glenn Research Center, Cleveland, Photovoltaic and Space Environments Branch, Cleveland, OH 44135, USA

Received 1 July 2004; received in revised form 1 September 2004; accepted 17 September 2004

Abstract

Copper indium disulfide (CuInS_2) films were deposited by aerosol-assisted chemical vapor deposition (AACVD) from a single-source precursor (SSP), $(\text{PPh}_3)_2\text{Cu}(\text{SET})_2\text{In}(\text{SET})_2$. Various deposition parameters were explored to understand how they affect the crystallography, stoichiometry, and morphology of the deposited films and the quality of fabricated solar cells. Parameters explored included the deposition temperature, location of substrate within CVD reactor, precursor concentration in toluene carrier solvent, and post-deposition annealing in a S-rich atmosphere. CuInS_2 films have been fabricated into complete solar cells with the top-down composition of $\text{Al/ZnO:F/CdS/CuInS}_2/\text{Mo/glass}$ and the efficiency of 1.0% under simulated AM0 illumination.

Published by Elsevier B.V.

Keywords: CuInS_2 ; Single-source precursor; Chemical vapor deposition

1. Introduction

Low temperature ($<400^\circ\text{C}$) deposition techniques for thin film photovoltaic devices are of interest to enable the use of lightweight, flexible substrates. Such devices provide a higher power-to-weight ratio and significant cost savings compared to current technologies. The National Aeronautics and Space Administration (NASA) is particularly interested in thin film technologies due to low launching costs, deployment and stowage options, radiation hardness, and potentially mission enabling benefits of such technologies [1].

The alloys of $\text{Cu}(\text{In,Ga})(\text{S,Se})_2$ have shown particularly high potential as thin film photovoltaic absorber layers [2,3] and $\text{Cu}(\text{In,Ga})\text{Se}_2$ based solar cells with conversion efficiencies as great as 19.2% in AM1.5 illumination have been cre-

ated [3]. The 1.45 eV direct band gap of CuInS_2 is near ideal for single junction devices in AM0 illumination [4] and has yielded cells conversion efficiencies as high as 11.4% [5] without the concerns for the toxicity of Se.

We have synthesized organometallic single-source precursors (SSPs) for chemical vapor deposition (CVD) to supply the required elements for chalcopyrite thin films at temperatures below 400°C [6]. The deposition of CuInS_2 films with good optical, morphological, and electrical properties via aerosol-assisted CVD (AACVD) of SSP has been previously demonstrated [7–10]. However, further optimization of this deposition process is required to improve film properties and cell performance.

AACVD is a common technique for achieving the advantages of both metal-organic CVD (MOCVD) and spray pyrolysis. AACVD offers benefits of a low temperature solution reservoir, as found in spray pyrolysis, and a uniform conformal film deposition with gas-phase precursors, as found in MOCVD techniques [11].

The intent of this paper is to characterize the CuInS_2 film deposition via AACVD. In contrast to previous studies that have aimed to show the feasibility of quality film deposition

* Corresponding authors. Tel.: +1 216 433 3540 (M.H.-C. Jin)/+1 216 433 3835 (A.F. Hepp); fax: +1 216 433 6106 (M.H.-C. Jin)/+1 216 433 6106 (A.F. Hepp).

E-mail addresses: michael.h.jin@grc.nasa.gov (M.H.-C. Jin), aloysius.f.hepp@nasa.gov (A.F. Hepp).

from SSPs and some characterization of the AACVD process [9,12], this paper seeks to further understand the deposition processes. The crystallographic, stoichiometric, and morphological characteristics of CuInS_2 films created in a variety of deposition parameters have been studied and have been used to better optimize the AACVD deposition process.

2. Experimental

CuInS_2 films were deposited by AACVD from a SSP, $(\text{PPh}_3)_2\text{Cu}(\text{SEt})_2\text{In}(\text{SEt})_2$. The precursor was prepared as previously reported elsewhere [6,13]. All moisture- or air-sensitive procedures were performed under Ar in a glove box or with standard Schlenk techniques. The precursor (1.5–3.5 g) was dissolved into distilled toluene (50–400 mL) and fed into the nebulizer via a syringe pump. A Sonaer Ultrasonics 2.4 MHz nebulizer atomized the precursor and solvent mixture and the aerosol was swept into the reactor via Ar carrier gas at a flow rate of 4 L/min. As shown in Fig. 1, the setup includes an atmospheric pressure, hot-wall horizontal reactor with a warm evaporation zone and a hot deposition zone, similar to that reported elsewhere [8,10].

As substrates, glass slides (Fisher catalog no. 12-550 A) were cut to approximately 9 mm by 76 mm and partially coated with Mo using a radio-frequency magnetron sputter. Small sections of each substrate were masked during Mo deposition so that CuInS_2 /glass could later be characterized. After Mo deposition, the substrates were placed on a susceptor within the CVD reactor tube for CuInS_2 deposition. The susceptor was solid graphite coated with SiC and modified to accommodate three substrates side by side at a 15.5° angle above horizontal, as shown in Fig. 1. The use of a susceptor in a reactor tube creates a variation between the ‘upstream’ and ‘downstream’ end of each substrate. The upstream end is closer to the evaporation zone and the bottom wall of the reactor tube while the downstream end is deeper within the deposition zone and closer to the axial center of the reactor tube.

Some deposited CuInS_2 films were subjected to post-deposition annealing. The annealing procedure consisted of placing the substrate and susceptor back into the deposition zone of the CVD reactor tube, setting the evaporation zone

temperature to 120°C and the deposition zone temperature to a temperature between 450 and 580°C , and flowing Ar through the reactor tube at a rate of 10 mL/min. The reactor ramped up to annealing temperatures from room temperature over 0.5 h and post annealing cooled to room temperature over 1 h. The anneal durations was recorded from when the substrate reached the set temperature to when it started cooling and ranged from 15 min to 17 h. Occasionally, anneals were performed in an excess of sulfur vapor. The sulfur was added via a sulfur powder filled crucible to the downstream side of the evaporation zone.

Optimization of this deposition procedure involved multiple parameters. Parameters manipulated in this study include the (1) temperature of the deposition zone, (2) location of the susceptor within the reactor tube, (3) concentration of the precursor within the solvent, and (4) post-deposition annealing. The effects of parameter variations were shown in the resulting CuInS_2 film properties.

CuInS_2 films were characterized by scanning electron microscopy (SEM, Hitachi S-3000N), energy dispersive spectroscopy (EDS, EDAX), profilometry (Dektak II), X-ray diffraction (XRD, Philips X’pert), and UV–vis transmission spectroscopy (Perkin-Elmer Lambda-19). Transmission spectroscopy and EDS data were obtained from film/glass sections of the upstream edge of each sample because the upstream CuInS_2 films were generally smoother and denser than the downstream sections. The film thickness for smooth films was determined by examination of the interference pattern of the transmission spectroscopy data as described by Swanepoel [14]. Well-adhering CuInS_2 films were etched in a 1.5 KCN solution and fabricated into solar cells with the top-down composition of Al/ZnO:F/CdS/ CuInS_2 /Mo/glass, as reported by Jin et al. [15]. Device properties were determined by the examination of current versus voltage characteristics obtained under simulated AM0 illumination.

3. Results and discussion

3.1. Film variations

CuInS_2 film morphologies were controlled by the deposition parameters to be (1) a smooth, shiny, dense film with

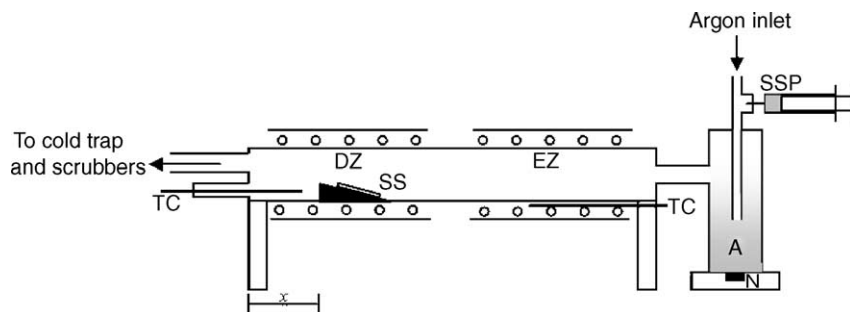


Fig. 1. Diagram of hot-wall aerosol-assisted chemical vapor deposition reactor. Shown are the single-source precursor and solvent (SSP), aerosol of precursor and solvent (A), nebulizer (N), evaporation zone (EZ), deposition zone (DZ), substrate and susceptor (SS), and thermocouples (TC). The position of the susceptor within the deposition zone is indicated by the variable x .

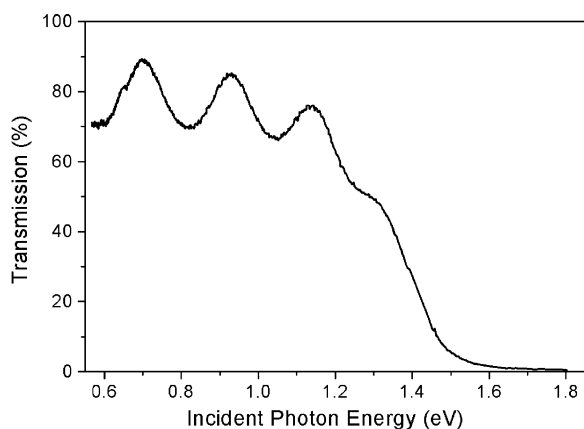


Fig. 2. Graph of transmission through CuInS₂ film on glass slide vs. energy of incident light.

bluish tint and excellent adherence or (2) a rough, dull, highly porous, dark black film with poor adherence. A gradual transition exists between these deposition regimes where CuInS₂ films with hazy, patchy, and/or gray appearance were created.

The downstream section of a substrate is more likely to be porous and adhere worse than the upstream sections due to variations in the concentration boundary layer through the reactor tube. As the precursor concentration in the Ar carrier gas decreases along the reactor tube, the thickness of the concentration boundary layer increases and the reaction is encouraged to exist in a more diffusion-limited state. The precursor must diffuse through the boundary layer to interact with the substrate, which is a longer distance at the downstream end of the substrate compared to the upstream end of the substrate [16].

Rough surface morphologies commonly occur in diffusion-limited reactions. Any variation in a substrate texture results in a non-uniform concentration boundary layer across the substrate. A small protrusion existing on a flat substrate in a diffusion-limited deposition will experience a greater precursor diffusion rate and consequently grow faster than the flat substrate regions. This cycle in diffusion-limited depositions encourages film roughness and high film porosity [17].

Characteristic transmission spectroscopy data are presented in Fig. 2. The thin film interference is evident for pho-

ton energies less than the 1.45 eV band gap for this smooth, dense film. The film thickness and index of refraction has been calculated through examination of the interference pattern [14] to yield values of 1.2 and 2.45 μm , respectively.

SEM images of the observed deposition morphologies are shown in Fig. 3. Fig. 3(a) shows a rough CuInS₂ film with greater porosity and larger features than the smooth CuInS₂ films, as shown in Fig. 3(b). Rough films were deposited in a more diffusion-limited regime with high porosity while smooth films were deposited in a less diffusion-limited regime with smaller grain size and higher film density. Evidence implicating these deposition rate-limiting factors is given in the following sections.

3.2. Deposition zone temperature

The deposition zone temperature was varied between 350 and 425 °C. The temperature variations altered the CuInS₂ film stoichiometry (Fig. 4(a)) and crystalline orientation (Fig. 4(b)) while not significantly affecting the deposition rate (Fig. 4(c)).

As shown in Fig. 4(a), EDS measurements indicate that increasing deposition zone temperatures yield increased S content in the deposited films. The ratio of Cu-to-In contained in the deposited films varies between 0.79 and 0.98, with the maximum occurring at 395 °C. No precursor residue was identified within the CuInS₂ films, implying a clean decomposition of the precursor into the building block for the CuInS₂ films at all deposition zone temperatures explored. Deposited films were closest to stoichiometric when deposited at 395 °C.

Further, the crystalline structure of the deposited CuInS₂ film was affected by the deposition zone temperature. The two common crystalline textures of CuInS₂ films are (1 1 2) and (2 2 0)/(2 0 4). Decreased series resistance was reported for cells obtained from CuInS₂ absorbers with a (1 1 2) crystalline orientation compared to those with (2 2 0)/(2 0 4) orientation [18]. As shown in the XRD data of Fig. 4(b), the deposition temperature affected the crystalline structure such that deposition temperatures around 395 °C produced the most preferred (1 1 2) orientation compared to both higher and lower deposition temperatures.

At a precursor delivery rate of 1.6 g/h, the film deposition rate was not regularly affected by the deposition tempera-

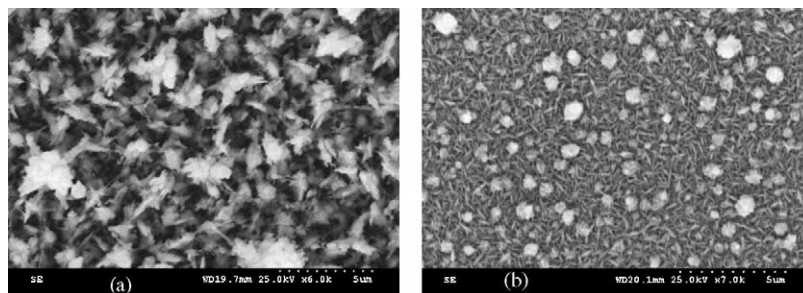


Fig. 3. SEM images of CuInS₂ films. Film morphologies include (a) porous, rough, black films and (b) smooth, shiny, dense films.

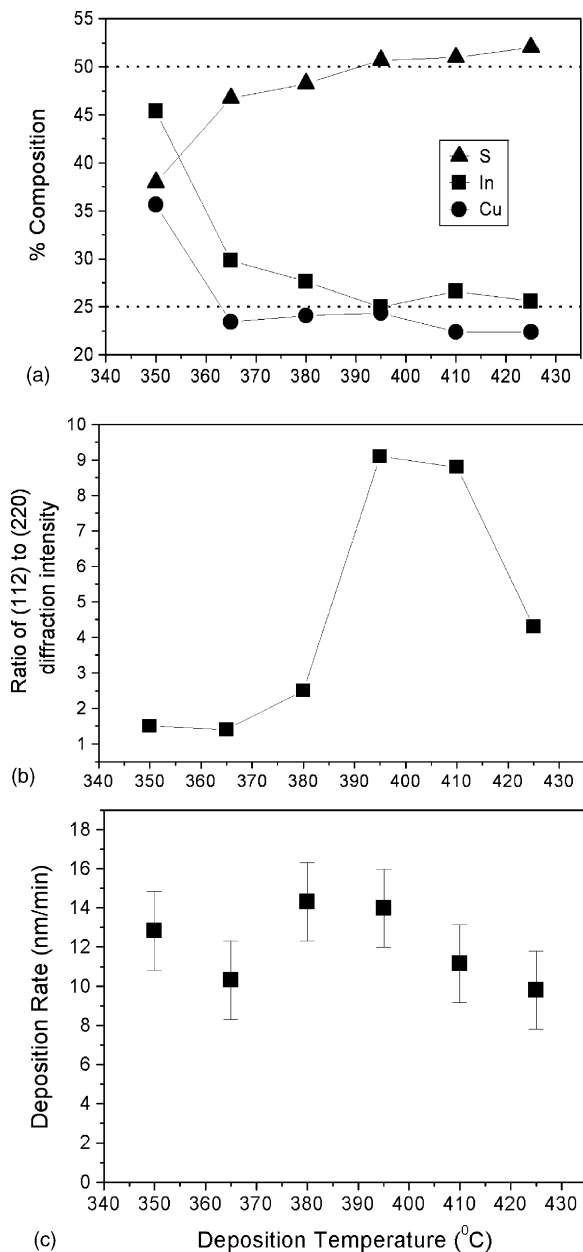


Fig. 4. Graphs of deposition temperature vs. (a) elemental composition, (b) crystalline orientation, and (c) deposition rate for CuInS₂ films with a precursor feed rate of 1.6 g/h. The error bars in (c) are the result from calculated film thickness from transmission spectroscopy interference patterns [14].

ture throughout the explored temperature range. As shown in Fig. 4(c), the film deposition rate was 12 ± 2 nm/min regardless of deposition temperature. This shows that the deposition rate was not limited by the thermal energy for the reaction and the deposition rate was not reaction-limited.

3.3. Precursor concentration in carrier solvent

Variations in the concentration of the SSP within toluene carrier solvent have been explored through the range of 0.005–0.04 mol/L. The precursor concentration affects the

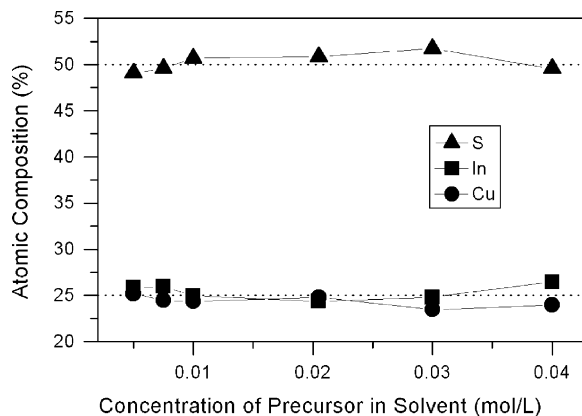


Fig. 5. Graph of elemental composition of CuInS₂ thin films vs. precursor concentration in toluene carrier solvent.

feed rate of the precursor into the reactor and the gas-phase density of the precursor within the reactor tube. The Ar carrier gas flow rate, nebulizing rate, and reactor setup also affect the precursor feed rate and gas-phase precursor density, although these variables were held constant throughout this study.

By increasing the concentration of precursor within toluene, the CuInS₂ deposition becomes less diffusion-limited and resulting films change from highly porous and rough to smooth and dense. As shown in Fig. 5, the precursor in toluene concentration does not noticeably affect the stoichiometry of the deposited films.

3.4. Susceptor and substrate location

Variations in the location of the susceptor have been studied at a substrate temperature of 395 °C. As shown in Fig. 6, the location of the susceptor did not significantly affect the elemental composition of the deposited film; films were near stoichiometry regardless of tested susceptor location.

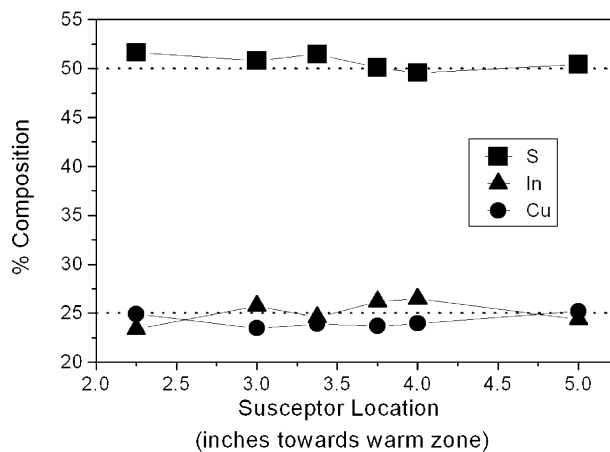


Fig. 6. Graph of elemental composition of CuInS₂ thin films vs. the susceptor location within the deposition zone. The location of the susceptor is indicated by the variable x, as shown in Fig. 1.

The location of the susceptor does influence the morphology of the deposited films. As the susceptor was moved towards the evaporation zone, the deposited film became denser and has better adhesion as a result of the varying concentration boundary layer through the reactor tube. Moving the susceptor towards evaporation zone exposes the substrate to a reduced concentration boundary layer that results in a less diffusion-limited reaction, throughout the range explored.

3.5. Post-deposition annealing

Post-deposition annealing was shown to beneficially affect the CuInS_2 film elemental composition and crystalline structure. During a 5 h, 580°C anneal without the inclusion of S, a CuInS_2 film's elemental composition of S, In, and Cu changed from 51.5, 24.5, and 24.0, respectively, to 51.0, 26.0, and 23.0%. However, by annealing for 5 h at 580°C in a S-rich atmosphere the CuInS_2 films elemental composition of S, In, and Cu changed to 52.0, 23.5, and 24.5%, respectively. Although these changes in elemental composition were within a typical standard deviation ($\pm 5\%$) of the analysis of EDS data without a reference sample, qualitatively consistent compositional changes were observed for anneal profiles of various length and temperature. For the film annealed under S-rich atmosphere, the precipitation of copper sulfide phase was not detected by XRD and there was no clear signature of compositional change after etching in a 1.5 M KCN solution for 1 min. A higher Cu-to-In ratio is preferable for CuInS_2 [19] and increased S content passivates S vacancies that are undesirable n-type dopants [20]. Thus, annealing in the presence of S beneficially changes the elemental composition of the CuInS_2 film.

The crystalline structure of CuInS_2 thin films often shows two polymorphs, chalcopyrite and meta-stable sphalerite, differing in the degree of order for the Cu and In atoms within the zinc-blende structure. The ordering of the Cu and In can be identified through characteristic XRD diffracting peaks and peak splitting which are only observed for the more ordered chalcopyrite structure [21]. Post-deposition annealing of CuInS_2 films increased the ordering of the Cu and In atoms within the crystalline structure and the structure became more ordered chalcopyrite. Confirmation of the chalcopyrite structure was seen most clearly from a film annealed at 580°C for 5 h (the longest anneal attempted at 580°C) in a S-rich Ar atmosphere, as shown in Fig. 7. The (1 0 1) and (2 1 1) diffractions, respectively, at 17.9° and 37.3° are particularly clear, as the peak splitting in the (2 0 0)/(0 0 4) and (1 1 6)/(3 1 2) diffractions at $32.2/32.4^\circ$ and $54.8/55.1^\circ$, none of which can exist in the pure sphalerite structure.

3.6. Solar cells

The solar cell efficiency achieved so far from our AACVD deposited CuInS_2 absorber is 1.03%, as shown in Fig. 8. The CuInS_2 film in this cell was smooth, dense, and annealed at 450°C for 17 h in an S-rich Ar atmosphere. A second cell

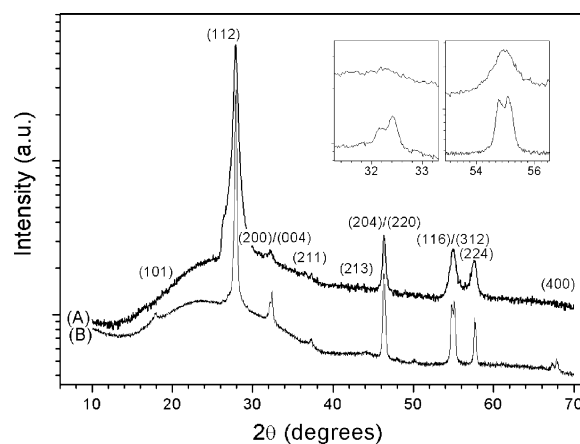


Fig. 7. Graph of typical XRD diffraction patterns from (A) as deposited and (B) annealed CuInS_2 films.

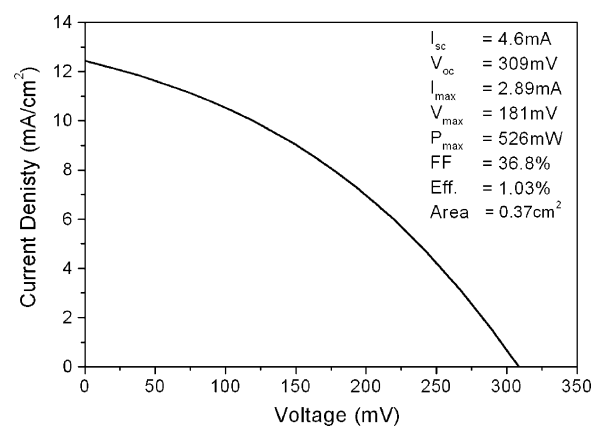


Fig. 8. CuInS_2 solar cell characteristics.

was fabricated from a separate smooth and dense CuInS_2 film that was not annealed; its efficiency is 0.92%. These cells show that annealing may improve cell performance, but annealing is not mandatory to achieve electrical response to illumination.

The low cell efficiencies were likely caused by the combination of a high series resistance and a low shunt resistance. The high series resistance could be the effect of poorly functioning individual layers or poor contacts between the layers. The low shunt resistance is likely due to a leaky junction between CuInS_2 absorber and a CdS layer.

4. Conclusion

CuInS_2 films were deposited via AACVD at low temperatures ($<400^\circ\text{C}$) from a SSP, $(\text{PPh}_3)_2\text{Cu}(\text{SET})_2\text{In}(\text{SET})_2$. CuInS_2 films were modified by the control of various deposition parameters, including the deposition temperature, susceptor location, and precursor concentration. Deposition control has produced films with two distinct morphologies, varying in density, adhesion, smoothness, and color. Addi-

tionally, post-deposition annealing in S-rich Ar atmosphere enhanced CuInS₂ film stoichiometry and crystalline structure. EDS analysis indicated that as-deposited and annealed films were near stoichiometric. XRD analysis showed clear chalcopyrite indicative diffractions for sulfur-annealed films. Devices fabricated from the CuInS₂ absorbers deposited at 395 °C, have efficiencies above 1.0%.

Acknowledgements

The authors gratefully acknowledge NASA for financial support cooperative agreement, NCC3-947. We also wish to thank Mr. David Scheiman from Ohio Aerospace Institute for his assistance with the solar simulator at NASA Glenn Research Center.

References

- [1] D.J. Hoffman, T.W. Kerslake, A.F. Hepp, M.K. Jacobs, D. Ponnusamy, Proceedings of the AIAA 35th Intersociety Energy Conversion Engineering Conference, Las Vegas, NV, July 2000, p. 670.
- [2] J. Klaer, I. Luck, K. Siemer, R. Klenk, D. Braunig, Proceedings of the 28th IEEE Photovoltaic Specialists Conference, Anchorage, AK, September 2000, p. 559.
- [3] K. Romanathan, M.A. Contreras, C.L. Perkins, S. Asher, F.S. Haseen, J. Keane, D. Young, M. Romero, W. Metzger, R. Noufi, J. Ward, A. Duda, Prog. Photovolt: Res. Appl. 11 (2003) 225.
- [4] W. Schockley, H.J. Queisser, J. Appl. Phys. 32 (1961) 510.
- [5] J. Klaer, I. Luck, A. Boden, R. Klenk, I.G. Perez, R. Scheer, Thin Solid Films 431/432 (2003) 534.
- [6] K.K. Banger, M.H.-C. Jin, J.D. Harris, P.E. Fanwick, A.F. Hepp, Inorg. Chem. 42 (2003) 7713.
- [7] K.K. Banger, J.A. Hollingsworth, J.D. Harris, J. Cowen, W.E. Buhro, A.F. Hepp, Appl. Organomet. Chem. 16 (2002) 617.
- [8] J.A. Hollingsworth, K.K. Banger, M.H.-C. Jin, J.D. Harris, J.E. Cowen, E.W. Bohannan, J.A. Switzer, W.E. Buhro, A.F. Hepp, Thin Solid Films 431/432 (2003) 63.
- [9] J.A. Hollingsworth, A.F. Hepp, W.F. Buhro, Chem. Vapour Depos. 5 (1999) 105.
- [10] J.D. Harris, K.K. Banger, D.A. Scheiman, M.A. Smith, M.H.-C. Jin, A.F. Hepp, Mater. Sci. Eng. B 98 (2003) 150.
- [11] T.T. Kodas, M. Hampden-Smith, Aerosol Processing of Materials, Wiley-VCH, New York, 1999, p. 537.
- [12] J.A. Hollingsworth, Ph.D. Thesis, Washington University, 1999.
- [13] K.K. Banger, J. Cowen, A.F. Hepp, Chem. Mater. 13 (2001) 3827.
- [14] R. Swanepoel, J. Phys. E 216 (1983) 1214.
- [15] M.H.-C. Jin, K.K. Banger, C.V. Kelly, J.H. Scofield, J.S. McNatt, J.E. Dickman, A.F. Hepp, Proceedings of the Space Photovoltaic Research and Technology Conference, #####, September 2003.
- [16] T.T. Kodas, M.J. Hampden-Smith, The Chemistry of Metal CVD, VCH, New York, 1994, p. 470.
- [17] C.H.J. van den Brekel, Philips Res. Rep. 32 (1997) 118.
- [18] K. Siemer, J. Klaer, I. Luck, D. Braunig, Proceedings of the 28th IEEE Photovoltaic Specialists Conference, Anchorage, AK, September 2000, p. 630.
- [19] S. Siebentritt, Thin Solid Films 403/404 (2002) 1.
- [20] H.Y. Ueng, H.L. Hwang, J. Phys. Chem. Solids 50 (1989) 1297.
- [21] J. Alvarez-Garcia, A. Perez-Rodriguez, A. Romano-Rodriguez, J.R. Morante, L. Calvo-Barrio, R. Scheer, R. Klenk, J. Vac. Sci. Technol. A 19 (2001) 232.